frontiers | Frontiers in Cellular and Infection Microbiology

TYPE Brief Research Report
PUBLISHED 24 February 2025
DOI 10.3389/fcimb.2025.1515779

OPEN ACCESS

EDITED BY
Muhammad Hafeez,
Agricultural Research Service (USDA),
United States

REVIEWED BY
Tejeshwar Rao,
University of Houston, United States
Iman Haghani,
Mazandaran University of Medical Sciences,
Iran

*CORRESPONDENCE
Natalia Schiefermeier-Mach
Natalia.schiefermeier-mach@fhg-tirol.ac.at

RECEIVED 23 October 2024
ACCEPTED 05 February 2025
PUBLISHED 24 February 2025

CITATION
Schiefermeier-Mach N, Polleux J, Heinrich L, Lechner L, Vorona O and Perkhofer S (2025) Biological boundary conditions regulate the internalization of *Aspergillus fumigatus* conidia by alveolar cells.
Front. Cell. Infect. Microbiol. 15:1515779.
doi: 10.3389/fcimb.2025.1515779

Biological boundary conditions regulate the internalization of *Aspergillus fumigatus* conidia by alveolar cells

Natalia Schiefermeier-Mach*, Julien Polleux, Lea Heinrich, Lukas Lechner, Olexandra Vorona and Susanne Perkhofer

Research and Innovation Unit, Health University of Applied Sciences Tyrol, FH Gesundheit Tirol, Innsbruck, Austria

Introduction: The lung environment is defined by unique biological boundary conditions, including complex alveolar geometry, extracellular matrix composition and mechanical forces generated during respiration. These factors were shown to regulate alveolar permeability, surfactant secretion, cell contractility and apoptosis, but their role in fungal infections remains unknown. *Aspergillus fumigatus* is a critical fungal pathogen that causes severe pulmonary infections in immunocompromised individuals. Our study addresses a knowledge gap by investigating how boundary conditions affect *A. fumigatus* conidia interactions with alveolar epithelial cells.

Methods: We applied micropatterned substrates to confine cells into defined shapes and densities, allowing precise control over geometric conditions and extracellular matrix composition. Using cell line stably expressing the phagolysosomal protein Lamp1-NeonGreen and multiplane fluorescent microscopy, we evaluated *A. fumigatus* conidia binding and internalization efficiency.

Results: We observed significantly faster and more efficient *A. fumigatus* conidia internalization in cells confined on micropatterns compared to previously reported studies using cell monolayers. Altering cell geometry, density and extracellular matrix composition strongly affected conidia binding and localization to Lamp1$^+$ phagolysosomes. Cells on X-shaped or multicellular micropatterns showed higher internalization rates, particularly at the periphery, suggesting spatial heterogeneity in pathogen uptake. Additionally, changes in extracellular matrix composition influenced the intracellular trafficking of *A. fumigatus* conidia.

Discussion: Our findings emphasize the essential role that local mechanical and biochemical cues play in shaping the interactions between fungal pathogens and alveolar cells. Understanding how lung boundary conditions change in disease states will provide important insights into fungal infection outcomes.

KEYWORDS

boundary conditions, micropatterning, geometric constraints, alveolar cells, *Aspergillus fumigatus*, host-pathogen interactions

1 Introduction

Biological boundary conditions are the physical and biochemical constraints that define the cellular environment and regulate cellular responses. These conditions include cell number, shape, size, extracellular matrix (ECM) composition, substrate stiffness and intercellular forces (Vahey and Fletcher, 2014). Investigating boundary conditions is important for understanding how cells interact with their environment and how these interactions influence their function. They have been shown to regulate essential cellular processes, such as adhesion, migration, proliferation, endocytosis, and bacteria-cell binding (Wickström et al., 2010; Hamidi et al., 2020; Bastounis et al., 2022; Wang et al., 2022; Feng et al., 2023; Isomursu et al., 2024).

Micropatterned substrates have provided important insights into how geometric constraints affect cellular functions (Azioune et al., 2010; Muoth et al., 2016; Wickström and Niessen, 2018; van der Putten et al., 2022). Confining cells to specific shapes alters their biomechanical properties, including cytoskeletal organization and focal adhesion dynamics, consequently influencing intracellular signaling pathways (Schauer and Goud, 2014; He et al., 2015). For example, cells on circular micropatterns exhibit distinct polarization patterns regulated by mechanical forces, like shear stress and tension (He et al., 2015). Schauer and Goud (Schauer and Goud, 2014) showed that geometric constraints alter endocytic activities, leading to asymmetric uptake of transferrin and epidermal growth factor ligands. Biological boundary conditions have been also suggested to determine the fate of internalized molecules and microorganisms (Muoth et al., 2016; Bastounis et al., 2022).

The role of boundary conditions is particularly relevant in host-pathogen interactions, where they can regulate pathogen survival within tissues. Previous research has shown that bacterial pathogens such as *Listeria monocytogenes* and *Shigella flexneri* exploit host-cell mechanics to spread by manipulating mechanical forces at cell-cell junctions and altering intracellular tension (Bastounis et al., 2022). Furthermore, Feng et al. recently showed that the initial adhesion of *Staphylococcus aureus* and *Escherichia coli* to host cells can be modulated by altering ECM rigidity and geometric constraints (Feng et al., 2023). Although this study evaluated bacteria attachment on host cells under biological constraints, the role of boundary conditions in fungal pathogen-host interactions, including internalization process, remains unexplored representing a critical gap in understanding infection mechanisms. Fungal infections cause over 3.8 million deaths annually, with *Aspergillus* species responsible for the highest mortality rates among fungal diseases (Denning, 2024). *Aspergillus fumigatus* is recognized as one of the top four critical fungal pathogens by the WHO (WHO Antimicrobial Resistance Division, 2022). These saprotrophic fungi produce dense clouds of conidia containing up to 10^8 spores per cubic meter. In healthy individuals, conidia are cleared in the airway by innate immune mechanisms including mucociliary clearance and macrophage phagocytosis (Latgé, 2001). However, in immunocompromised individuals, compromised immune defenses allow *A. fumigatus* to survive in the lungs, causing various forms of pulmonary aspergillosis, ranging from mild hypersensitivity to severe invasive infections (Dagenais and Keller, 2009; Vanderbeke et al., 2018; Latgé and Chamilos, 2019).

Interaction between lung cells and *A. fumigatus* conidia is a complex process that involves both professional phagocytic cells and non-professional phagocytes like alveolar epithelial cells (Wasylnka and Moore, 2002, 2003). Although phagocytic cells are more efficient, alveolar cells can also internalize conidia, potentially leading to their destruction (Wasylnka et al., 2005; Jia et al., 2023). Some conidia may still survive, ultimately re-entering the extracellular space and contributing to persistent infection (Wasylnka and Moore, 2003; Croft et al., 2016; Culibrk et al., 2019). Understanding how lung-specific boundary conditions influence conidia internalization will provide new insights into fungal infection mechanisms.

In this study, we developed an *in vitro* model to investigate the interactions between *A. fumigatus* conidia and alveolar epithelial cells using micropatterning techniques. This approach allowed us to evaluate how key features of alveolar boundary conditions affect conidia binding, internalization and intracellular trafficking. By addressing this knowledge gap, our work provides a novel perspective on the influence of lung-specific microenvironments on fungal infections. We demonstrate that the internalization and intracellular processing of fungal conidia are significantly influenced by cell density, geometry and ECM composition. Expanding this approach to other pathogens could uncover novel mechanisms of infection and identify new targets for therapeutic intervention.

2 Materials and methods

2.1 Fungal strains and growth conditions

A. fumigatus DAL (wild-type, CBS 144.89) strain was cultured in filter-cap cell culture bottles on sabouraud 4% glucose agar (15 g/L agar, 40 g/L D (+)-glucose, 10 g/L peptone, Sigma-Aldrich, 1.06404, Austria) at 37°C for 10 days until full maturation of conidia was observed. Conidia were collected by plate flooding using sterile spore buffer (0.01% Tween, Fisher Scientific, 10113103, Germany, 0.9% NaCl, Carl Roth, 8986.1, Germany), centrifugated at 4000 rpm for 5 minutes and resuspended in sterile spore buffer.

2.2 Cell culture

Human A549 cell line stably expressing Lamp1-NeonGreen (Schiefermeier-Mach et al., 2021) were cultured in a growth medium consisting of RPMI-1640 (Capricorn, RPMI-XA, Germany), 10% fetal bovine serum (FBS, Capricorn Scientific, FBS-11A, Germany), 2 µl/ml puromycin, (Carl Roth, 0240.2, Germany) 1% penicillin/streptomycin (Capricorn Scientific, PS-B, Germany) and 1% L-glutamine (Capricorn Scientific, GLN-B, Germany).

2.3 Culturing cells on coverslips with micropatterns

Micropatterns were generated with deep-ultraviolet (UV) lithography on polyethylene glycol (PEG)-coated glass coverslips. Glass coverslips were incubated in a 1 mM solution of a linear PEG-

silane (Rapp Polymere – reference 122000-71, Germany) in dry toluene for 20 h at 80°C under inert atmosphere, in order to covalently immobilize a monolayer of PEG (Azioune et al., 2010; Clausen et al., 2023). The substrates were removed, rinsed intensively with isopropanol, methanol and water, and dried with nitrogen. A PEG-coated glass coverslip and a chromium-coated quartz photomask (Compugraphics, Jena) were assembled with a vacuum on a holder, which was immediately exposed to deep ultraviolet (UV) light using a low-pressure mercury lamp (NIQ 60/35 XL longlife lamp, quartz tube, 60 W from Heraeus Noblelight, Germany) at 5 cm distance for 5 min. Deep UV light with a wavelength of 185 nm oxidizes PEG, significantly impairs PEG antifouling properties and allows ECM protein adsorption. The patterned substrates were subsequently incubated with 150 µl of fibronectin (10 µg/ml, Sigma Aldrich, 341631, Austria) in PBS or vitronectin (3.3 µl/ml, ProSci, 91-362, USA) at 4°C overnight and washed once with PBS. 1 ml of growth medium containing 10^5 cells/ml (for smaller micropatterns) or 10^6 cells/ml (for bigger micropatterns) was added and incubated in growth medium with reduced FCS (1%) for 2 hours at 37°C to allow adhesion. Cells were further carefully washed with warm PBS to remove unattached cells and further incubated in growth medium with reduced FCS (1%) overnight.

2.4 Infection with *A. fumigatus* conidia

For infection experiments, cells were grown in 35 mm culture dishes on fibronectin- or vitronectin-coated micropatterns in serum-reduced medium and incubated for 24 hours. After the incubation time, the serum-reduced medium was carefully replaced with fresh RPMI-1640 containing 10% FBS without antibiotics. Cells were infected with 10^6 cfu/ml *A. fumigatus* conidia. Infected cells were incubated for 1 and 3 hours at 37°C prior to fixation.

2.5 Fluorescence microscopy

Cells infected with *A. fumigatus* conidia were fixed as described before with slight modifications (Scheffler et al., 2014). In short, 8% paraformaldehyde (PFA, Sigma Aldrich, 104005, Austria) in PBS was slowly added directly to the cells in cell medium in proportion 1:1 and incubated for 15 minutes at 37°C. Then, medium-PFA mix was carefully replaced with 4% PFA, incubated further 15 minutes and washed with PBS. Cells were further incubated with a mixture of EasyProbe ™ ActinRed 555 to visualize actin (THP Medical Products, FP032, Austria), Dapi (Sigma-Aldrich, D9542-5MG, Austria, 1:4000) for nuclei staining and 0.05% saponin in PBS for 1 hour at room temperature following washing in PBS and mounting on glass objective slides with Mowiol (Sigma-Aldrich, C9368, Austria).

All images were taken using an inverted wide-field IX83 Olympus Microscope (Olympus Austria) equipped with UPlanXApo 60x, 1.42 N.A, PH3 objective and 2x digital zoom. Images were recorded in fluorescence (Dapi, TRITC, FITC) and phase contrast (PH3) channels as multiplane Z-stacks with a step size set for all images at 0,5 µm. A resolution of 2048 x 2048 and a 16-bit-grayscale were used. Images were further de-convoluted using cellSens software (Olympus, deconvolution parameters: nearest neighbor 50%). For TRITC/FITC fluorescence channels exposure times of 120-150 ms, for Dapi 8 ms and phase contrast (PH3) 60ms were applied. 50 micropatterns from 3 biological repetitions were analyzed for each data set. Manual analysis of images was performed independently by two trained scientists using the "Point tool" and "Analyze-Measure" functions in Fiji software (RRID: SCR_002285). Quantifications of the center of mass of fungal conidia, as well as $Lamp1^+$ and a subpopulation of $Lamp1^+Actin^+$ were saved as X, Y-coordinates. Z-stacks were examined in parallel: Dapi staining was used to count the cell number, a multi-channel merged fluorescence image of FITC/TRITC channels was used to identify $Lamp1^+$ and $Lamp1^+Actin^+$ vesicles, phase contrast images were used to quantify the total number of conidia and for the identification of co-localization with Lamp1-NeonGreen and actin.

2.6 Image quantification and statistical analysis

Analysis was performed in GraphPad Prism 10.1.2 (RRID: SCR_002798, USA) and figures were prepared in Fiji and Adobe Photoshop (RRID: SCR_014199). Tests used: descriptive statistics, ordinary one-way ANOVA (multiple comparisons), correlation analysis (correlation matrix, with Pearson coefficients, two-tailed, 95% confidence interval). The statistical significance of the data was determined by p-values.

3 Results

3.1 Micropattern size and cell density regulate *A. fumigatus* conidia binding and internalization

To investigate the influence of cell confinement on the internalization of *A. fumigatus* conidia, human A549 cells stably expressing Lamp1-NeonGreen were cultured on fibronectin-coated circular micropatterns of 28 µm and 60 µm in diameter. We used circular patterns of different sizes to minimize cell contractility in contrast to non-micropatterned substrates and X-shaped patterns. By increasing pattern diameter, cell density was increased and cell area decreased, leading further to changes in cell contractility. To obtain a reproducible cell density, suspended single cells were seeded on patterns for only 2 hours to avoid the formation of cellular aggregates and multilayers on individual patterns. Upon

washing unbound cells, adhered cells were further cultured overnight to give them time to form a homogeneous monolayer, similar to an epithelial monolayer.

Cells were seeded at various densities to achieve 1 and 2 cells on smaller micropatterns and 10-12 cells on bigger patterns (Figure 1A). The defined cell geometry or grouping of cells on each micropattern facilitated the quantification and mapping of host-pathogen interaction events by overlaying conidia coordinates from 50 identical micropatterns. Lamp1-NeonGreen was used as a marker of conidia internalization into phagolysosomes (Schiefermeier-Mach et al., 2021). Infection of cells with dormant *A. fumigatus* conidia for 1 and 3 hours resulted in specific conidia adhesion to confined cells without binding to the PEG-coated surrounding area. The average total number of detected conidia was significantly higher on big micropatterns with multicellular islands in comparison to smaller ones and strongly increased over time. However, there were no differences for 28 µm-micropattern with 1 or 2 cells (Figure 1B).

Multiplane imaging of cells by phase contrast and fluorescence microscopy revealed that some conidia were internalized into phagolysosomes (Lamp1$^+$ vesicles) already after 1 hour, (Figure 1C; Supplementary Video S1). Since cells on micropatterns of different sizes can bind different numbers of conidia per pattern, we further normalized all values to the "total number of conidia" for each individual micropattern condition for better comparisons. Quantification of conidia in Lamp1$^+$ vesicles as a part of all observed conidia showed a higher percentage on multicellular islands of 60 µm in diameter as compared to cells on 28 µm-patterns. Moreover, this percentage increased over time. Interestingly, not only the micropattern size but the number of cells per micropattern correlated with the number of phagolysosomes. There were significantly more conidia in Lamp1$^+$ vesicles when 2 cells were confined to 28 µm-patterns in comparison to 1 cell (Figure 1D).

Further analysis of conidia distribution revealed that binding and phagolysosomal internalization of conidia were heterogeneously distributed across the micropattern (Figure 1E). Conidia mapping and their radial distribution showed that their binding and internalization at the outer edge of the 60 µm-patterns is favored. A similar trend for 28 µm-patterns with 2 cells was also observed. The lowest number of conidia was detected in the center of all micropatterns independent of size and cell number (Figures 1E, F).

3.2 Cell density influences conidia trafficking in a subpopulation of Lamp1$^+$Actin$^+$ vesicles

To further investigate the intracellular trafficking and processing of *A. fumigatus* conidia, we additionally stained infected cells with an actin probe to detect intracellular actin distribution. We have observed that a small subset of Lamp1$^+$ vesicles containing fungal conidia also displayed actin, forming a Lamp1$^+$Actin$^+$ subpopulation (Figure 2A). The proportion of conidia within these double-positive vesicles was relatively small compared to the overall Lamp1$^+$ vesicles. However, the percentage of Lamp1$^+$Actin$^+$ vesicles relative to the total conidia number, showed a significant increase of these vesicles in 28 µm-patterns harboring 2 cells as compared to 1 cell or 10-12 cells on larger micropatterns (Figure 2B). Interestingly, in contrast to the population of Lamp1$^+$ vesicles, which increased over time, the percentage of conidia in double-positive vesicles remained stable between 1 and 3 hours (Figure 2B). Conidia mapping further showed the number and localization of double vesicles with a tendency toward micropattern edges on bigger micropatterns (Figure 2C).

3.3 ECM composition impacts conidia binding, internalization and trafficking in micropatterned cells

Next, we assessed the impact of ECM substrates in our cell model. We analyzed multicellular island constrained on 60 µm - micropattern coated with vitronectin (VN) instead of fibronectin (FN). VN is known from the literature to preferentially recruit ß3 integrins whereas FN recruits more ß1 integrins to coordinate cell adhesion (Schaufler et al., 2016). Analysis of conidia distribution on cells constricted on 60 µm-patterns coated with VN, revealed that binding and phagolysosomal internalization of conidia were similarly to the ones on FN (Supplementary Figure S1A). With both coating conditions, more binding and internalization of conidia was observed at the outer edge of the micropattern (Supplementary Figures S1A, B). When we quantified the average total number of conidia, we observed a decrease when using VN versus FN (Figure 2D). However, the percentage of conidia internalized in the Lamp1$^+$ vesicles did not differ from the one observed in cells micropatterned on FN (Figure 2D). Interestingly, there was a strong difference between the substrates in terms of the percentage of conidia internalized into the subpopulation of Lamp1$^+$Actin$^+$ vesicles: this percentage was increased when cells were constrained on VN (Figure 2D).

3.4 Cell shape and cell number impact conidia distribution and internalization in cells constricted on X-shaped micropatterns

To further investigate the impact of cell geometry on the cell-conidia interactions, we seeded A549-Lamp1-NeonGreen cells on X-shaped patterns with an edge of 28 µm. By presenting edges and adhesion-free areas, X-shaped patterns allowed us to further modify cell contractility and investigate its effect on conidia internalization. By varying the number of cells, we established 3 distinct cell densities: 1, 2 and 4 cells per micropattern, each resulting in characteristic changes in cell morphology due to the shape constraints imposed by the X-pattern (Figure 3A). Upon infection with *A. fumigatus* conidia for 1 and 3 hours, we observed notable differences in conidia internalization across these conditions. Similarly to circular patterns, conidia were heterogeneously distributed across the micropattern with increased binding and

10.3389/fcimb.2025.1515779

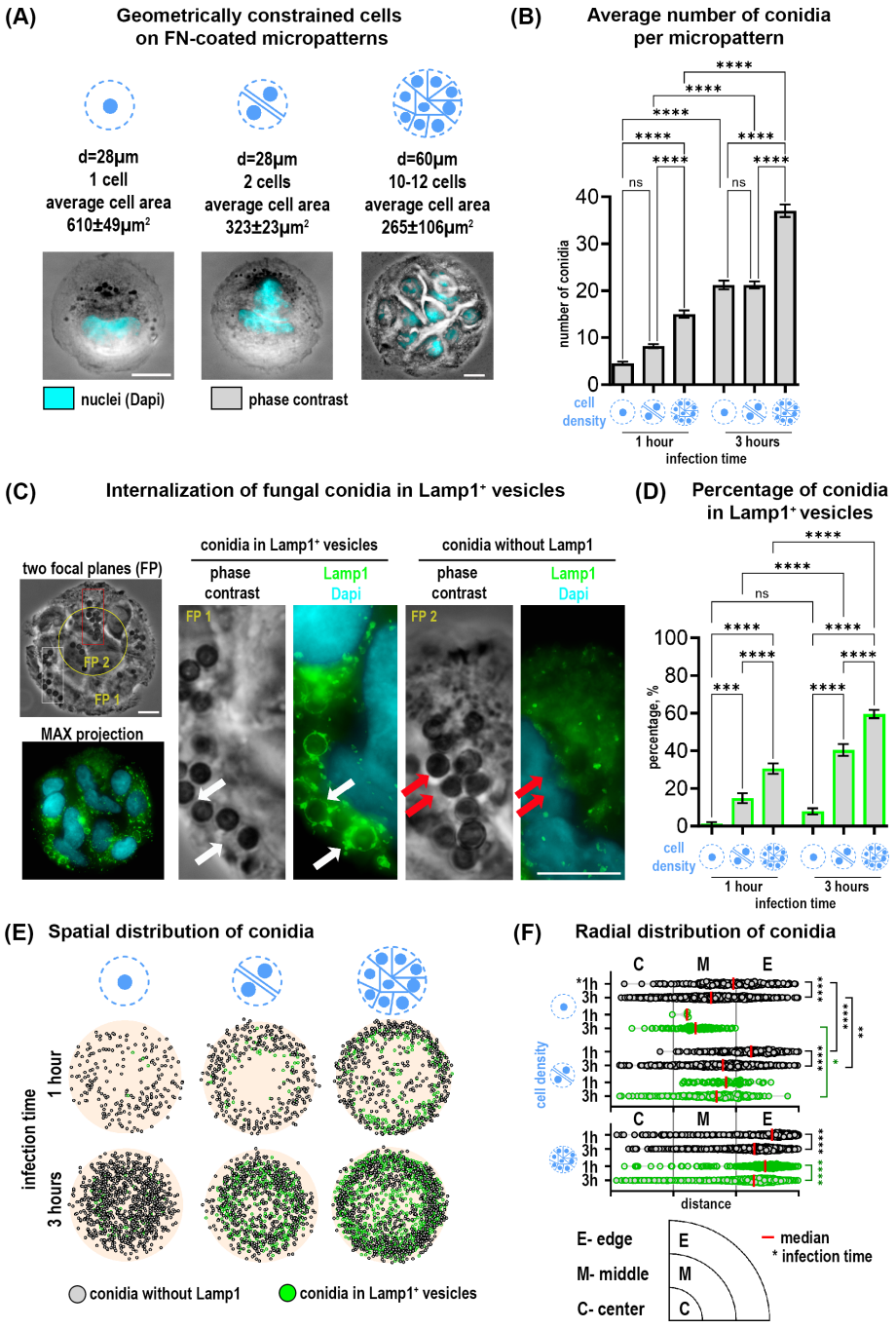

FIGURE 1
Distribution and internalization of *A fumigatus* conidia in A549 cells constrained on fibronection-coated circular micropatterns. **(A)** Representative images of cells constrained on micropatterns with diameters of 28 µm and 60 µm, and different cell densities. **(B)** Quantification of the average number of total conidia per micropattern at 1 and 3 hours post-infection. **(C)** Conidia internalization into phagolysosomes after 1 hour post-infection (Lamp1$^+$ vesicles). Phase contrast image includes two focal planes superposed. The overview of Lamp1 distribution is shown as the maximal Z-projection of FITC/Dapi channels of 9 focal planes (MAX projection). Magnified images show conidia in Lamp1$^+$ vesicles (white arrows) and conidia without Lamp1 signal (red arrows). **(D)** Percentage of conidia internalized in Lamp1$^+$ vesicles relative to the total conidia number at 1 and 3 hours post-infection. **(E)** Conidia spatial distribution map of 50 overlaid micropatterns displaying Lamp1$^+$ vesicles with internalized conidia (green spheres) and conidia without Lamp1 signal (grey spheres). **(F)** The radial distribution of conidia defined as the distance between the micropattern center and the center of a single conidia. These distances were grouped into three segments (center, middle and edge of pattern). Depicted are conidia without Lamp1 (grey spheres) and conidia in Lamp1$^+$ vesicles (green spheres). *P≤ 0.05; **P ≤ 0.01; ***P ≤ 0.001; ****P ≤ 0.0001; ns P > 0.05. FP, focal plane; FN, fibronectin. Scale bars = 10 µm. See also Supplementary Video 1.

10.3389/fcimb.2025.1515779

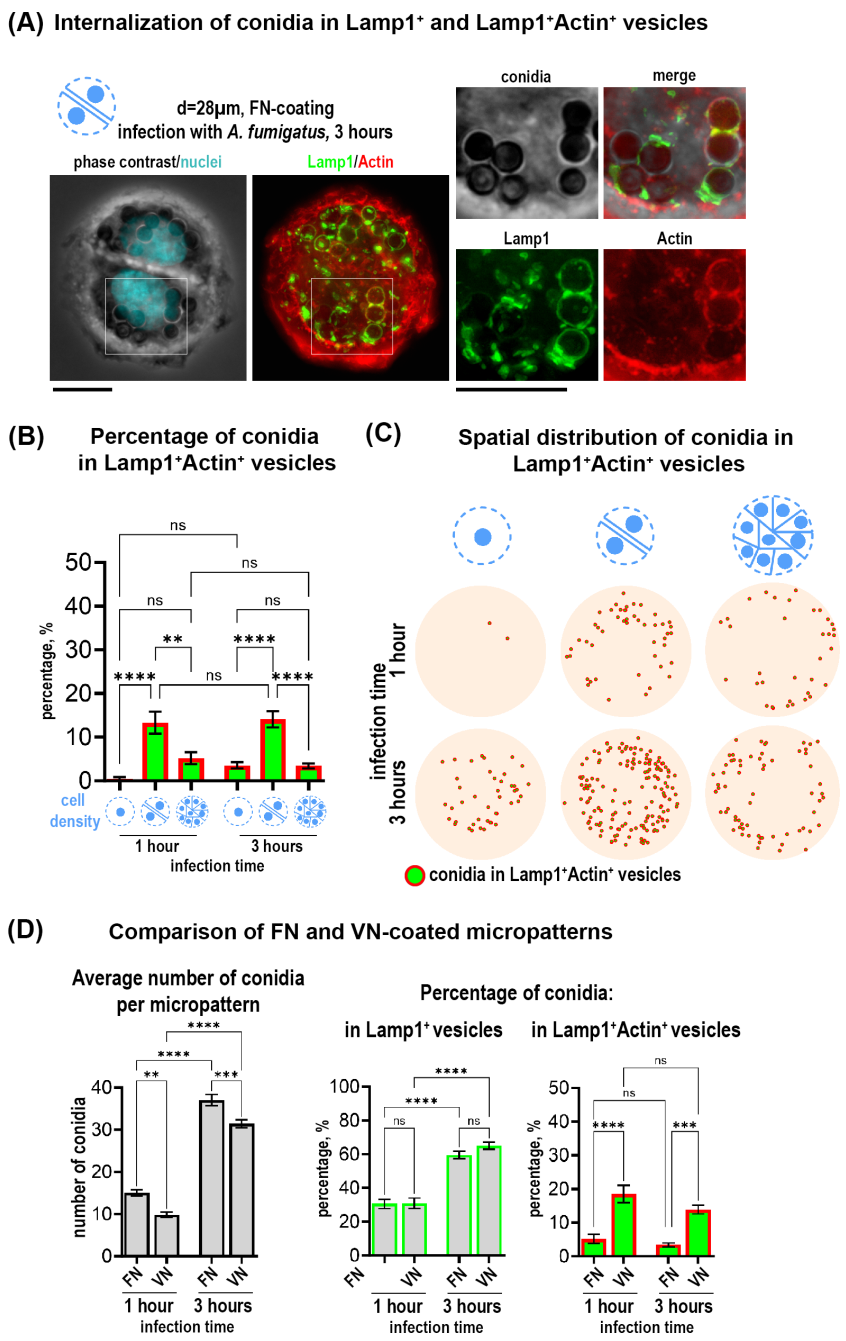

FIGURE 2
Internalization of *A fumigatus* conidia in a subpopulation of Lamp$^+$Actin$^+$ vesicles in cells on circular micropatterns and effect of ECM composition on conidia internalization. **(A)** Representative example of two cells on fibronectin-coated circular micropattern (28 µm). Overview of Lamp1 and Actin is shown as maximal Z-projection of FITC/TRITC channels of 9 focal planes. Magnified images show conidia in Lamp1$^+$ (green) and Lamp1$^+$Actin$^+$ vesicles (red and green) 3 hours post-infection. Scale bars = 10 µm. **(B)** Percentage of conidia internalized in Lamp1$^+$Actin$^+$ vesicles relative to the total conidia number in cells constrained on fibronectin-coated circular micropatterns with different sizes and cell density at 1 and 3 hours post-infection. **(C)** Conidia spatial distribution map of 50 overlaid micropatterns displaying Lamp1$^+$Actin$^+$ vesicles with internalized conidia (green spheres in red circles). **(D)** Comparison of vitronectin- and fibronectin micropatterns. Quantification of the average number of total conidia and the percentage of conidia internalized in Lamp1$^+$ and Lamp1$^+$Actin$^+$ vesicles at 1 and 3 hours post-infection relative to the total conidia number. **P ≤ 0.01; ***P ≤ 0.001; ****P ≤ 0.0001; ns P > 0.05. VN, vitronectin; FN, fibronectin. See also Supplementary Figure 1.

internalization at the outer edge (Figures 3B, C). After 1 hour of infection, while the average total number of conidia did not differ, there was an increased percentage of conidia in Lamp1$^+$ vesicles in the 4-cell configuration in comparison to 1 cell and 2 cells (Figures 3D, E). After 3 hours of infection, the average total number of conidia correlated with cell number and was the highest in the 4-cell micropattern. Internalization of conidia in Lamp1$^+$ vesicles increased after 3 hours compared to 1 hour and was higher in micropatterns with 2 and 4 cells compared to those with only 1 cell. The percentage of conidia in double Lamp1$^+$Actin$^+$

10.3389/fcimb.2025.1515779

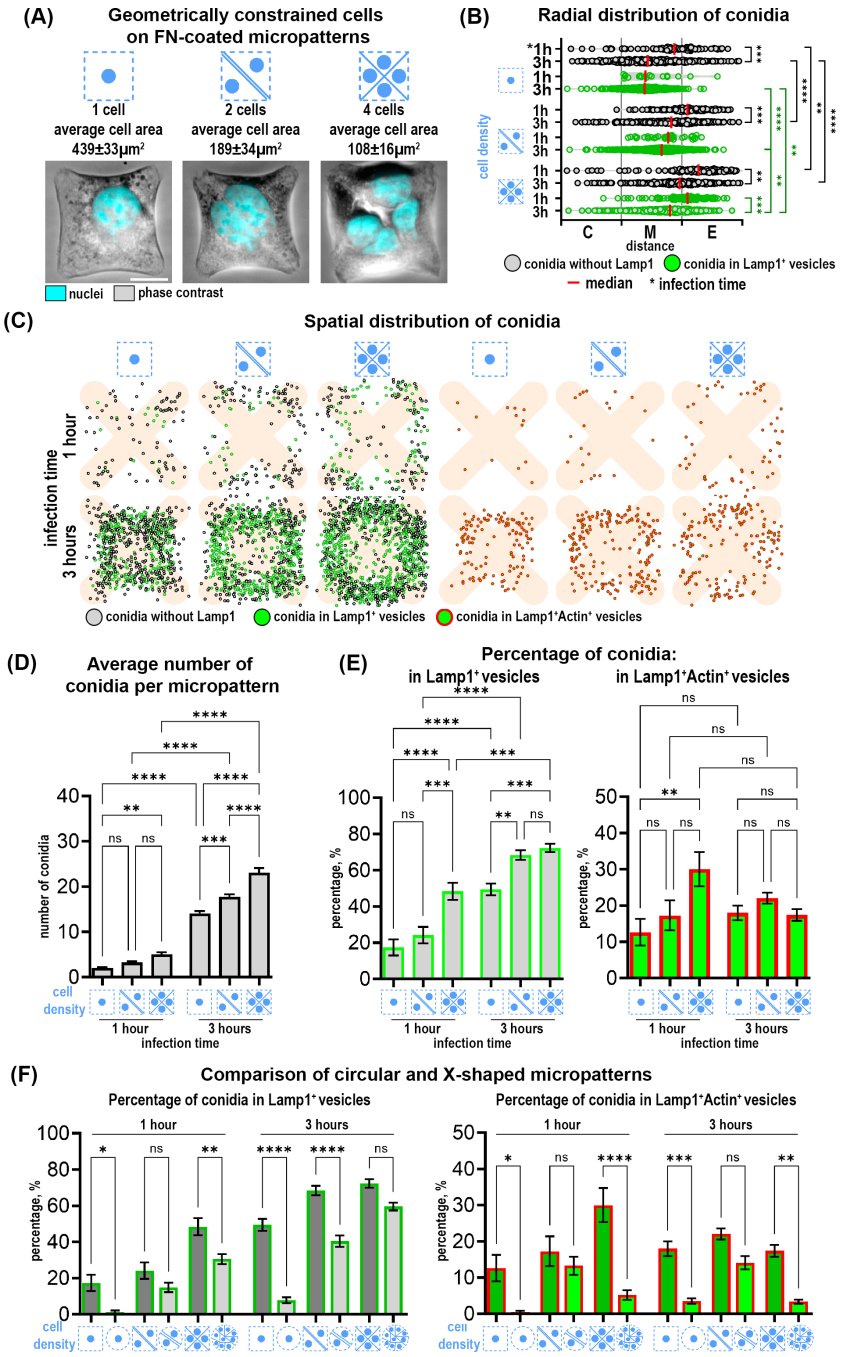

FIGURE 3
Distribution and internalization of *A fumigatus* conidia in A549 cells constrained on fibronectin-coated X-shaped micropatterns. **(A)** Representative phase contrast images of cells constrained on X-micropatterns with different cell densities. FN- fibronectin. Scale bars = 10 μm. **(B)** The radial distribution of conidia defined as the distance between the micropattern center and the center of a single conidia. These distances were grouped into three segments (center, middle and edge of pattern). Depicted are conidia without Lamp1 (grey spheres) and conidia in Lamp1$^+$ vesicles (green spheres). **(C)** Map of conidia spatial distribution in 50 overlaid micropatterns showing Lamp1$^+$ vesicles with internalized conidia (green spheres), conidia without Lamp1 signal (grey spheres) and conidia in Lamp1$^+$Actin$^+$ vesicles (green spheres in red circles). **(D)** Quantification of the average number of total conidia. **(E)** Percentage of conidia internalized in Lamp1$^+$ and in Lamp1$^+$Actin$^+$ vesicles at 1 and 3 hours post-infection relative to the total conidia number. **(F)** Comparison of the percentage of conidia internalized in Lamp1$^+$ and Lamp1$^+$Actin$^+$ vesicles in cells confined on X-shaped and circular micropatterns. *P≤ 0.05; **P ≤ 0.01; ***P ≤ 0.001; ****P ≤ 0.0001; ns P > 0.05.

vesicles did not differ significantly between the X-micropatterns with different cell numbers and did not change over time.

Interestingly, there were notable differences when comparing X-shaped to circular micropatterns (Figure 3F). Conidia were internalized more efficiently by cells constrained on X-micropatterns. Moreover, the percentage of double Lamp1$^+$Actin$^+$ vesicles was also higher in these cells (Figure 3F). To further elucidate the relationship between different parameters and conidia internalization, we performed a correlation

analysis using a correlation matrix and Pearson correlation coefficients. This analysis revealed that the percentage of conidia in Lamp1$^+$ and Lamp1$^+$Actin$^+$ vesicles was negatively correlated with cell area at both 1 hour and 3 hours. This negative correlation was moderate after 1 hour (r=-0.447) and strong after 3 hours (r=-0.716). The correlation of cell area with Lamp1$^+$Actin$^+$ vesicles was negative and moderate both after 1 hour (r=-0.310) and 3 hours (r=-0.299). No other significant correlations with other parameters were found.

4 Discussion

Our study emphasizes the role of biological boundary conditions in the regulation of host-pathogen interactions in the lung. The complex geometry of the alveoli and the mechanical forces during respiration establish a unique environment that influences cellular behavior (Roan and Waters, 2011). Previous studies showed that cell geometry, ECM composition, and mechanical forces affect essential lung functions, including alveolar permeability (Cavanaugh et al., 2005), surfactant secretion (Edwards, 2001), and apoptosis (Hammerschmidt et al., 2007). Here, we extend this understanding by demonstrating that boundary conditions also regulate the binding, internalization and intracellular fate of *A. fumigatus* conidia in alveolar epithelial cells. Our data provided new insights into how the lung's microenvironment can influence infection outcomes, particularly under conditions of altered mechanical and biochemical cues.

The choice of micropatterns was particularly advantageous for our study as it allowed precise control over cell geometry, density, and ECM composition, simulating specific aspects of the alveolar environment. We observed that constraining cells on micropatterns strongly increased the efficiency of conidia binding and phagolysosomal internalization compared to previous studies with no cell confinement (Wasylnka and Moore, 2002; Jia et al., 2023), reaching up to 30% already after one hour of infection. Our results further showed that cell shape and density had profound effects on conidia uptake. Cells on X-shaped micropatterns demonstrated higher internalization efficiency compared to circular ones, suggesting that specific geometric configurations create environments more conducive to pathogen internalization. Previous studies in single cells showed that the size and shape of the micropattern influence contractility and actin organization (Pitaval et al., 2010; Théry, 2010). Cells on X-shaped micropatterns had regions of localized higher tension, since this shape forced them to stretch along the diagonals, increasing mechanical stress at intersections and edges (James et al., 2008). In circular patterns, cellular tension was more evenly distributed, but still higher at the periphery than the center (Théry et al., 2006; Théry and Bornens, 2006). Such control over cell mechanics and geometry is a significant benefit of using micropatterning techniques, enabling detailed investigation into how specific physical constraints can enhance or limit pathogen internalization.

In multicellular islands, micropatterns dictate not only individual cell behavior but also the collective dynamics of cell groups (Théry, 2010). Peripheral cells were observed to be more contractile compared to those in the center, with higher traction forces at the edges. This variation arose due to spatial confinement, leading to differences in cell proliferation and differentiation across the micropattern (Nelson et al., 2005; He et al., 2015; Lin et al., 2022; Nelson et al., 2024). Although larger single cells might theoretically offer more surface area for conidia binding, our results showed that smaller cells within multicellular islands internalized more conidia than larger, single cells. This was

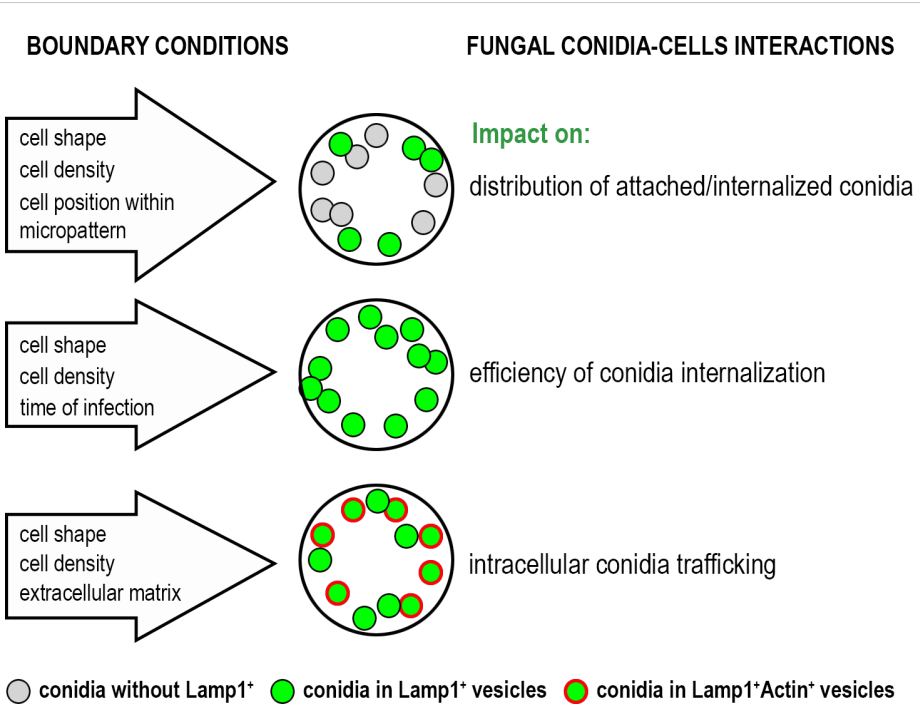

FIGURE 4
The impact of biological boundary conditions investigated in this study on the interactions of *A. fumigatus* conidia with alveolar cells.

significant on both circular and X-shaped micropatterns. The geometric constraint also affected the recruitment of actin to the phagolysosomal membranes. Cells on X-shaped micropatterns exhibited a higher frequency of $Lamp1^+Actin^+$ vesicles compared to circular ones. Interestingly, while the percentage of conidia in $Lamp1^+$ vesicles increased over the infection period, the percentage of $Lamp1^+Actin^+$ vesicles plateaued after one hour, suggesting that actin recruitment to phagolysosomes may be limited to specific stages of vesicle maturation.

Moreover, the binding and internalization events were more frequent at the periphery of the multicellular micropattern. This finding was consistent with the work of Feng et al (Feng et al., 2023), who showed that spatial tension heterogeneity leads to uneven collagen expression and increases bacterial adhesion at the periphery of micropatterned multicellular islands. Our results extended these observations to interactions with fungal pathogens. This phenomenon may be particularly relevant in the lung, where mechanical heterogeneity arises from alveolar geometry and the forces generated during respiration (Roan and Waters, 2011). In pathological conditions such as fibrosis or emphysema, where ECM stiffness is altered, these effects may be enhanced, potentially creating regions more susceptible to infection (Colebatch et al., 1973; Wilson, 1983).

Our findings also highlighted the influence of ECM composition on conidia internalization and trafficking. By varying coating substrates, distinct effects on conidia processing were observed. When cells were plated on vitronectin (VN), the integrin activation profile shifted from α5β1 (a main integrin for fibronectin (FN)) to αvβ3 integrin (Schaufler et al., 2016). This shift decreased overall conidia binding compared to FN-coating but increased the proportion of conidia internalized into $Lamp1^+Actin^+$ vesicles. These results suggested that integrin-mediated signaling pathways play a role in determining the fate of internalized conidia. It aligns with previous studies showing that different integrin receptors, specifically α5β1 and αvβ3, influence cytoskeletal dynamics, vesicular trafficking and phagocytosis (Dupuy and Caron, 2008; Bastounis et al., 2022). The increased presence of $Lamp1^+Actin^+$ vesicles in cells on VN substrate indicated that β3 integrin engagement may favor a trafficking pathway involving dynamic actin rearrangement, potentially facilitating more efficient phagosome maturation. The impact of biological boundary conditions on the *A. fumigatus* conidia- cells interactions is summarized in Figure 4.

In summary, our study emphasizes the significance of biological boundary conditions in shaping host-pathogen interactions. The heterogeneous internalization observed across different micropattern configurations suggests that some lung regions may be more prone to infection than others, especially during chronic disease states. This highlights the importance of spatially localized mechanical cues in determining the efficiency of conidia uptake and processing, with potential implications for understanding fungal infection establishment in the lung. Future research should aim to dissect the molecular mechanisms linking mechanical forces to pathogen internalization, particularly under varying disease conditions that alter ECM composition and stiffness or respiratory mechanics.

Data availability statement

The raw data supporting the conclusions of this article will be made available by the authors, without undue reservation.

Ethics statement

Ethical approval was not required for the studies on humans in accordance with the local legislation and institutional requirements because only commercially available established cell lines were used.

Author contributions

NS-M: Conceptualization, Funding acquisition, Supervision, Visualization, Writing – original draft, Writing – review & editing, Project administration, Resources. JP: Conceptualization, Methodology, Validation, Writing – original draft, Project administration, Resources, Writing – review & editing. LH: Formal analysis, Methodology, Validation, Visualization, Writing – original draft. LL: Formal analysis, Methodology, Visualization, Writing – original draft, Funding acquisition. OV: Formal analysis, Writing – original draft, Visualization. SP: Writing – original draft, Resources.

Funding

The author(s) declare financial support was received for the research, authorship, and/or publication of this article. This research was funded by Tirol Wissenschaftsfoerderung TWF to Natalia Schiefermeier-Mach (F.33484) and to Lukas Lechner (F.47867).

Conflict of interest

The authors declare that the research was conducted in the absence of any commercial or financial relationships that could be construed as a potential conflict of interest.

Generative AI statement

The author(s) declare that no Generative AI was used in the creation of this manuscript.

Publisher's note

Supplementary material

The Supplementary Material for this article can be found online at: https://www.frontiersin.org/articles/10.3389/fcimb.2025.1515779/full#supplementary-material

SUPPLEMENTARY FIGURE 1
Distribution and internalization of *A. fumigatus* conidia in A549 cells constrained on vitronectin-coated micropatterns. **(A)** Conidia spatial distribution map of 50 overlaid micropatterns displaying conidia without Lamp1 (grey spheres), conidia in Lamp1$^+$ vesicles (green spheres) and conidia in the subpopulation of Lamp1$^+$Actin$^+$ vesicles (green spheres in red circles). **(B)** The radial distribution of conidia defined as the distance between the micropattern center and the center of a single conidia. These distances were grouped into three segments (center, middle and edge of pattern). Depicted are conidia without Lamp1 (grey spheres) and conidia in Lamp1$^+$ vesicles (green spheres).

SUPPLEMENTARY VIDEO 1
Example of a Z-stack for Figure 1C. Z-stack with 19 focal planes of phase contrast channel (left) and merged FITC/Dapi fluorescent channels (right), magnification x60, scale bar =10 µm, the distance between focal planes =0.3 µm.

References

Azioune, A., Carpi, N., Tseng, Q., Théry, M., and Piel, M. (2010). Protein micropatterns: A direct printing protocol using deep UVs. *Methods Cell Biol.* 97, 133–146. doi: 10.1016/S0091-679X(10)97008-8

Bastounis, E. E., Radhakrishnan, P., Prinz, C. K., and Theriot, J. A. (2022). Mechanical forces govern interactions of host cells with intracellular bacterial pathogens. *Microbiol. Mol. Biol. Rev.* 86, e0009420. doi: 10.1128/mmbr.00094-20

Cavanaugh, K. J., Cohen, T. S., and Margulies, S. S. (2005). Stretch increases alveolar epithelial permeability to uncharged micromolecules. *Am. J. Physiol. Cell Physiol.* 290, C1179–C1188. doi: 10.1152/ajpcell.00355.2004

Clausen, B. E., Amon, L., Backer, R. A., Berod, L., Bopp, T., Brand, A., et al. (2023). Guidelines for mouse and human DC functional assays. *Eur. J. Immunol.* 53, e2249925. doi: 10.1002/eji.202249925

Colebatch, H. J., Finucane, K. E., and Smith, M. M. (1973). Pulmonary conductance and elastic recoil relationships in asthma and emphysema. *J. Appl. Physiol.* 34, 143–153. doi: 10.1152/jappl.1973.34.2.143

Croft, C. A., Culibrk, L., Moore, M. M., and Tebbutt, S. J. (2016). Interactions of aspergillus fumigatus conidia with airway epithelial cells: A critical review. *Front. Microbiol.* 7. doi: 10.3389/fmicb.2016.00472

Culibrk, L., Croft, C. A., Toor, A., Yang, S. J., Singhera, G. K., Dorscheid, D. R., et al. (2019). Phagocytosis of aspergillus fumigatus by human bronchial epithelial cells is mediated by the arp2/3 complex and WIPF2. *Front. Cell Infect. Microbiol.* 9. doi: 10.3389/fcimb.2019.00016

Dagenais, T. R. T., and Keller, N. P. (2009). Pathogenesis of aspergillus fumigatus in invasive aspergillosis. *Clin. Microbiol. Rev.* 22, 447–465. doi: 10.1128/CMR.00055-08

Denning, D. W. (2024). Global incidence and mortality of severe fungal disease. *Lancet Infect. Dis.* 24, e428–e438. doi: 10.1016/S1473-3099(23)00692-8

Dupuy, A. G., and Caron, E. (2008). Integrin-dependent phagocytosis: spreading from microadhesion to new concepts. *J. Cell Sci.* 121, 1773–1783. doi: 10.1242/jcs.018036

Edwards, Y. S. (2001). Stretch stimulation: its effects on alveolar type II cell function in the lung. *Comp. Biochem. Physiol. Part A: Mol. Integr. Physiol.* 129, 245–260. doi: 10.1016/s1095-6433(01)00321-x

Feng, Y., Wang, S., Liu, X., Han, Y., Xu, H., Duan, X., et al. (2023). Geometric constraint-triggered collagen expression mediates bacterial-host adhesion. *Nat. Commun.* 14, 8165. doi: 10.1038/s41467-023-43827-6

Hamidi, S., Nakaya, Y., Nagai, H., Alev, C., Kasukawa, T., Chhabra, S., et al. (2020). Mesenchymal-epithelial transition regulates initiation of pluripotency exit before gastrulation. *Development* (Cambridge, England) 147 (3), dev184960. doi: 10.1242/dev.184960

Hammerschmidt, S., Kuhn, H., Gessner, C., Seyfarth, H.-J., and Wirtz, H. (2007). Stretch-induced alveolar type II cell apoptosis: role of endogenous bradykinin and PI3K-Akt signaling. *Am. J. Respir. Cell Mol. Biol.* 37, 699–705. doi: 10.1165/rcmb.2006-0429OC

He, S., Liu, C., Li, X., Ma, S., Huo, B., and Ji, B. (2015). Dissecting collective cell behavior in polarization and alignment on micropatterned substrates. *Biophys. J.* 109, 489–500. doi: 10.1016/j.bpj.2015.06.058

Isomursu, A., Alanko, J., Hernández-Pérez, S., Saukkonen, K., Saari, M., Mattila, P. K., et al. (2024). Dynamic micropatterning reveals substrate-dependent differences in the geometric control of cell polarization and migration. *Small Methods* 8, e2300719. doi: 10.1002/smtd.202300719

James, J., Goluch, E. D., Hu, H., Liu, C., and Mrksich, M. (2008). Subcellular curvature at the perimeter of micropatterned cells influences lamellipodial distribution and cell polarity. *Cell Motil. Cytoskeleton* 65, 841–852. doi: 10.1002/cm.20305

Jia, L.-J., Rafiq, M., Radosa, L., Hortschansky, P., Cunha, C., Cseresnyés, Z., et al. (2023). Aspergillus fumigatus hijacks human p11 to redirect fungal-containing phagosomes to non-degradative pathway. *Cell Host Microbe* 31, 373–388.e10. doi: 10.1016/j.chom.2023.02.002

Latgé, J.-P., and Chamilos, G. (2019). Aspergillus fumigatus and Aspergillosis in 2019. *Clinical microbiology reviews*. 33 (1), e00140-18. doi: 10.1128/CMR.00140-18

Latgé, J.-P., and Chamilos, G. (2019). Aspergillus fumigatus and aspergillosis in 2019. *Clin. Microbiol. Rev.* 33. doi: 10.1128/CMR.00140-18

Lin, F., Zhou, Y., Duan, X., Fang, X., Zhang, Q., Zhang, Y., et al. (2022). Spontaneous formation and spatial self-organization of mechanically induced mesenchymal-like cells within geometrically confined cancer cell monolayers. *Biomaterials* 281, 121337. doi: 10.1016/j.biomaterials.2021.121337

Muoth, C., Rottmar, M., Schipanski, A., Gmuender, C., Maniura-Weber, K., Wick, P., et al. (2016). A micropatterning approach to study the influence of actin cytoskeletal organization on polystyrene nanoparticle uptake by BeWo cells. *RSC Adv.* 6, 72827–72835. doi: 10.1039/C6RA13782B

Nelson, C. M., Jean, R. P., Tan, J. L., Liu, W. F., Sniadecki, N. J., Spector, A. A., et al. (2005). Emergent patterns of growth controlled by multicellular form and mechanics. *Proc. Natl. Acad. Sci. U.S.A.* 102, 11594–11599. doi: 10.1073/pnas.0502575102

Nelson, C. M., Xiao, B., Wickström, S. A., Dufrêne, Y. F., Cosgrove, D. J., Heisenberg, C.-P., et al. (2024). Mechanobiology: Shaping the future of cellular form and function. *Cell* 187, 2652–2656. doi: 10.1016/j.cell.2024.04.006

Pitaval, A., Tseng, Q., Bornens, M., and Théry, M. (2010). Cell shape and contractility regulate ciliogenesis in cell cycle–arrested cells. *J. Cell Biol.* 191, 303–312. doi: 10.1083/jcb.201004003

Roan, E., and Waters, C. M. (2011). What do we know about mechanical strain in lung alveoli? *Am. J. Physiol. Lung Cell Mol. Physiol.* 301, L625–L635. doi: 10.1152/ajplung.00105.2011

Schauer, K., and Goud, B. (2014). Why does endocytosis in single cells care which side up? *Bioarchitecture* 4, 62–67. doi: 10.4161/bioa.28809

Schaufler, V., Czichos-Medda, H., Hirschfeld-Warnecken, V., Neubauer, S., Rechenmacher, F., Medda, R., et al. (2016). Selective binding and lateral clustering of α5β1 and αvβ3 integrins: Unraveling the spatial requirements for cell spreading and focal adhesion assembly. *Cell Adh. Migr.* 10, 505–515. doi: 10.1080/19336918.2016.1163453

Scheffler, J. M., Schiefermeier, N., and Huber, L. A. (2014). Mild fixation and permeabilization protocol for preserving structures of endosomes, focal adhesions, and actin filaments during immunofluorescence analysis. *Meth. Enzymol.* 535, 93–102. doi: 10.1016/B978-0-12-397925-4.00006-7

Schiefermeier-Mach, N., Moresco, V., Geley, S., Heinrich, L., Lechner, L., Oberhauser, H., et al. (2021). Evaluation of stable lifeAct-mRuby2- and LAMP1-neonGreen expressing A549 cell lines for investigation of aspergillus fumigatus interaction with pulmonary cells. *Int. J. Mol. Sci.* 22 (11), 5965. doi: 10.3390/ijms22115965

Théry, M. (2010). Micropatterning as a tool to decipher cell morphogenesis and functions. *J. Cell Sci.* 123, 4201–4213. doi: 10.1242/jcs.075150

Théry, M., and Bornens, M. (2006). Cell shape and cell division. *Curr. Opin. Cell Biol.* 18, 648–657. doi: 10.1016/j.ceb.2006.10.001

Théry, M., Racine, V., Piel, M., Pépin, A., Dimitrov, A., Chen, Y., et al. (2006). Anisotropy of cell adhesive microenvironment governs cell internal organization and orientation of polarity. *Proc. Natl. Acad. Sci. U.S.A.* 103, 19771–19776. doi: 10.1073/pnas.0609267103

Vahey, M. D., and Fletcher, D. A. (2014). The biology of boundary conditions: cellular reconstitution in one, two, and three dimensions. *Curr. Opin. Cell Biol.* 26, 60–68. doi: 10.1016/j.ceb.2013.10.001

Vanderbeke, L., Spriet, I., Breynaert, C., Rijnders, B. J. A., Verweij, P. E., and Wauters, J. (2018). Invasive pulmonary aspergillosis complicating severe influenza: epidemiology, diagnosis and treatment. *Curr. Opin. Infect. Dis.* 31, 471–480. doi: 10.1097/QCO.0000000000000504

van der Putten, C., Buskermolen, A. B. C., Werner, M., Brouwer, H. F. M., Bartels, P. A. A., Dankers, P. Y. W., et al. (2022). Correction to "Protein micropatterning in 2.5D: an approach to investigate cellular responses in multi-cue environments. *ACS Appl. Materials Interfaces* 14, 15859. doi: 10.1021/acsami.2c04641

Wang, Y., Wang, N., Yang, Y., Chen, Y., and Zhang, Z. (2022). Cellular nanomechanics derived from pattern-dependent focal adhesion and cytoskeleton to balance gene transfection of Malignant osteosarcoma. *J. Nanobiotechnol.* 20, 499. doi: 10.1186/s12951-022-01713-1

Wasylnka, J. A., Hissen, A. H. T., Wan, A. N. C., and Moore, M. M. (2005). Intracellular and extracellular growth of Aspergillus fumigatus. *Med. Mycol.* 43, S27–S30. doi: 10.1080/13693780400029247

Wasylnka, J. A., and Moore, M. M. (2002). Uptake of Aspergillus fumigatus Conidia by phagocytic and nonphagocytic cells *in vitro*: quantitation using strains expressing green fluorescent protein. *Infect. Immun.* 70, 3156–3163. doi: 10.1128/IAI.70.6.3156-3163.2002

Wasylnka, J. A., and Moore, M. M. (2003). Aspergillus fumigatus conidia survive and germinate in acidic organelles of A549 epithelial cells. *J. Cell Sci.* 116, 1579–1587. doi: 10.1242/jcs.00329

WHO Antimicrobial Resistance Division. (2022). *WHO fungal priority pathogens list to guide research, development and public health action*. Available online at: https://iris.who.int/bitstream/handle/10665/363682/9789240060241-eng.pdf?sequence=1 (Accessed September 11, 2024).

Wickström, S. A., Lange, A., Hess, M. W., Polleux, J., Spatz, J. P., Krüger, M., et al. (2010). Integrin-linked kinase controls microtubule dynamics required for plasma membrane targeting of caveolae. *Dev. Cell* 19, 574–588. doi: 10.1016/j.devcel.2010.09.007

Wickström, S. A., and Niessen, C. M. (2018). Cell adhesion and mechanics as drivers of tissue organization and differentiation: local cues for large scale organization. *Curr. Opin. Cell Biol.* 54, 89–97. doi: 10.1016/j.ceb.2018.05.003

Wilson, T. A. (1983). Nonuniform lung deformations. *J. Appl. Physiol. (1985)* 54, 1443–1450. doi: 10.1152/jappl.1983.54.6.1443